American Mineralogist, Volume 89, pages 1119–1129, 2004

An X-ray Rietveld study of piemontite on the join $Ca_2Al_3Si_3O_{12}(OH)$–$Ca_2Mn^{3+}_3Si_3O_{12}(OH)$ formed by hydrothermal synthesis

MARIKO NAGASHIMA* AND MASAHIDE AKASAKA

Department of Materials Creation and Circulation Technology, Interdisciplinary Graduate School of Science and Engineering, Shimane University, Matsue 690-8504, Japan

ABSTRACT

Mn^{3+} distribution at octahedral M1, M2, and M3 sites of piemontite and its effect on structural changes were investigated by X-ray Rietveld analysis of synthetic $Ca_2Al_{3-p}Mn^{3+}_pSi_3O_{12}(OH)$ piemontites. The material studied was synthesized from starting materials of $Ca_2Al_{3-q}Mn^{3+}_qSi_3O_{12.5} + H_2O$ in hydrothermal experiments with P_{fluid} of 200 and 350 MPa and temperature of 500 °C. Piemontites crystallized as single phases from $q = 0.5$, 0.75, 1.0, and 1.1 starting materials, whereas minor amounts of bixbyite and parawollastonite were associated with those synthesized from $q = 1.5$ and 1.75 starting materials. EPMA analyses of synthetic piemontites showed that the maximum Mn^{3+} content was 1.3(1) apfu. Site preference of Mn^{3+} at the octahedral sites is M3 > M1 >> M2. Mn^{3+} occupancies (g) at the M3 and M1 sites are correlated with the p-value in piemontite as $g^{M3} = -0.20p^2 + 1.00p$ and $g^{M1} = 0.23p^2 - 0.06p$, respectively, where $0.0 \le p \le 1.3$. With increasing p-value, the mean M3-O and M1-O distances of piemontites increase, but the M1-O1 distance and the O5-Si3-O6 angle change nonlinearly due to the Jahn-Teller effect. The nonlinear variations of the a and c parameters with increasing p are caused by changes in the M1-O1 distance and the O5-Si3-O6 angle, respectively. The M3 octahedra, which are more distorted than the M1 octahedra, become more tetragonally compressed with increasing Mn^{3+} at the M3 site, due to the substantial increase of the M3-O1 distance.

INTRODUCTION

Piemontite, an epidote group mineral, occurs in metamorphic rocks and manganiferous ore deposits subjected to low- to moderate-temperature metamorphism at very high oxygen fugacity and low CO_2 partial pressure. It is also a late crystallization product in some acid and intermediate lavas.

The main components of most natural piemontites are $Ca_2Al_3Si_3O_{12}(OH)$, $Ca_2Mn^{3+}_3Si_3O_{12}(OH)$, and $Ca_2Fe^{3+}_3Si_3O_{12}(OH)$. Ca^{2+} cations occupy nine-coordinated A1 and 10-coordinated A2 sites; Al, Mn^{3+}, and Fe^{3+} cations are distributed among octahedral M1, M2, and M3 sites, and Si cations occur in the tetrahedral site. The octahedral sites form two types of chains of edge-sharing octahedra: a single chain of the M2 octahedra and a multiple chain of central M1 and peripheral M3 octahedra (Ito et al. 1954; Dollase 1968, 1969).

The distribution of Mn^{3+} and Fe^{3+} in the three types of octahedral sites and the structural changes caused by (Mn^{3+},Fe^{3+}) substitution for Al in epidote group minerals have been investigated in terms of single crystal structure refinements (Dollase 1969, 1971; Kvick et al. 1988; Ferraris et al. 1989; Bonazzi et al. 1990, 1992; Bonazzi and Menchetti 1994, 1995; Langer et al. 2002; and others). The crystal chemistry of natural epidote group minerals including piemontite has also been investigated using a variety of spectroscopic methods (Burns and Strens 1967; Dollase 1973; Paesano et al. 1983; Fehr and Heuss-Assbichler 1997; Langer et al. 2002; and others). However, since natural piemontites commonly contain not only Mn^{3+} but also Fe^{3+} in the octahedral sites and other larger cations such as Sr, REE, and Mn^{2+} in the A2 and/or A1 sites, it has been difficult to investigate the influence of Mn^{3+} substitution for Al on the structural changes.

Anastasiou and Langer (1977) synthesized $Ca_2Al_{3-p}Mn^{3+}_pSi_3O_{12}(OH)$-piemontites at 1.5 GPa and 800 °C, and studied their structural changes in terms of the variation of unit-cell parameters caused by the substitution of Mn^{3+} for Al. They determined a maximum p-value of about 1.9, and proposed discontinuities of the unit-cell parameters near $p = 1$. Single-crystal structure refinements of synthetic piemontites with $p = 0.83$, 0.98, and 1.47 synthesized at 1.5 GPa and 800 °C were carried out by Langer et al. (2002). However, as noted by Langer et al. (2002), their single crystal data for synthetic piemontites were too few to confirm the breaks in unit-cell parameters near $p = 1$. Piemontite with $p = 1.0$ has also been synthesized successfully at lower pressures and temperatures than those used by Anastasiou and Langer (1977): e.g., at 200 MPa and 500–650 °C (Strens 1964; Keskinen and Liou 1979, 1987), and 200–300 MPa and 500–600 °C (Akasaka et al. 2000, 2003). However, maximum Mn^{3+} content in $Ca_2Al_3Si_3O_{12}(OH)$–$Ca_2Mn^{3+}_3Si_3O_{12}(OH)$ piemontite and the crystal structures of the piemontites synthesized at these conditions have not yet been investigated.

In our study, we investigated the solubility of the $Ca_2Mn^{3+}_3Si_3O_{12}(OH)$-component and the crystal structures of $Ca_2Al_3Si_3O_{12}(OH)$–$Ca_2Mn^{3+}_3Si_3O_{12}(OH)$ piemontites synthesized at 200–350 MPa and 500 °C to compare them to the piemontites synthesized at higher pressures and temperatures by Anastasiou and Langer (1977) and Langer et al. (2002). In this paper, we report the results of piemontite synthesis from $Ca_2Al_{3-q}Mn^{3+}_qSi_3O_{12.5} + H_2O$ starting materials of $q = 0.5$, 0.75,

* E-mail: s039707@matsu.shimane-u.ac.jp

1.0, 1.1, 1.5, and 1.75, the X-ray powder structural refinements of these synthetic piemontites, and interpret the variations of unit-cell parameters caused by Mn^{3+} substitution for Al in terms of interatomic distances and angles.

Experimental methods

Strens (1964), Keskinen and Liou (1979), and Akasaka et al. (2000) successfully synthesized piemontites using oxide mixtures as starting materials. Consequently, we employed oxide mixtures as starting materials for the piemontite synthesis. Strens (1964) synthesized well-grown piemontite crystals from glass starting material at 200 MPa and 500 °C using natural seed crystals. However, in our preliminary work, we were unable to synthesize large piemontite crystals from glass starting material, and garnet was associated with the piemontite that did form (Akasaka et al. 2000). Each reagent-grade chemical was treated as follows: $CaCO_3$ and MnO_2 were heated at 110 ºC for 3 hours, Al_2O_3 was heated at 1100 ºC for 3 hours, and SiO_2 was heated at 1350 ºC until amorphous silica was transformed to cristobalite. Appropriate amounts of $CaCO_3$, Al_2O_3, MnO_2, and SiO_2 were mixed to produce compositions of $Ca_2Al_{3-q}Mn^{3+}_qSi_3O_{12.5}$, where q = 0.5, 0.75, 1.0, 1.1, 1.5, and 1.75. The mixtures were heated at 850 ºC in air for one hour to break down the carbonate. MnO_2 was also converted to Mn_2O_3 by this treatment. Complete decomposition of the carbonate and conversion of MnO_2 to Mn_2O_3 were confirmed by X-ray powder diffraction analysis of the heated starting materials.

The starting materials were sealed in $Ag_{90}Pd_{10}$ capsules with excess distilled water. The solid oxygen buffer technique was employed to produce f_{O_2} adequate to maintain manganese in the trivalent state. An Mn_2O_3/MnO_2 oxygen buffer was used, based on published studies of piemontite syntheses by Strens (1964), Anastasiou and Langer (1977), Keskinen and Liou (1979), and Akasaka et al. (2000).

Our hydrothermal syntheses were carried out at P_{fluid} of 200 and 350 MPa and temperatures of 500 and 550 °C, using standard cold-seal pressure vessels. Temperatures were measured by chromel-alumel thermocouples. Experimental pressures and temperatures are accurate to within ±5 MPa and ±5 °C, respectively.

Experimental products were identified using X-ray powder diffractometry (Cu$K\alpha$ radiation). Chemical compositions of the synthetic phases were analyzed using a JEOL JXA-8800M electron probe microanalyzer operated at 15 kV, with a beam current of 20 nA and beam diameter of 1 µm. Standards used were natural wollastonite for Ca and Si, synthetic MnO for Mn, and synthetic Al_2O_3 for Al. The ZAF method was used for data correction. The oxidation state of Mn in synthetic piemontites was determined from the relative intensities of the $L\alpha$ and $L\beta$ X-ray emission peaks (Albee and Chodos 1970; Kimura and Akasaka 1999). Those intensities were measured with the instrument operating at 15 kV, using a TAP crystal (Kimura and Akasaka 1999).

Grinding samples to a very small particle size is one of the most critical requirements for any structure study based on powder X-ray diffraction data (Bish and Reynolds 1989; Post and Bish 1989). To achieve this, samples were finely ground under alcohol in a hand agate mortar and pestle until resultant particle sizes were less than 5 µm. Powdered samples were mounted in glass sample holders with 20 × 15 × 0.2 mm or 20 × 15 × 0.5 mm cavities. Mounts for intensity profile collection were made by loading the powder from the front of the holder. Following the method of Raudsepp et al. (1990), a straightedge was used to level the sample surface to that of the holder. The surface was then finely serrated several times with a razor blade. This technique tends to randomize the orientation of anisotropic crystals that are aligned during filling, while maintaining a generally flat surface.

Step-scan powder diffraction data were collected using a RIGAKU RINT automated X-ray powder diffractometer using a Bragg-Brentano goniometer equipped with incident- and diffracted-beam soller slits, 1° divergence and anti-scatter slits, a 0.15 mm receiving slit, and a curved graphite diffracted-beam monochrometer. The normal-focus Cu X-ray tube was operated at 35 kV and 25 mA. Profiles were taken between 10° and 150° 2θ with a step interval of 0.04° 2θ, using step counting times that accumulated around five thousand counts for the strongest peaks.

Crystal structures of synthetic piemontites were refined using the RIETAN-2000 program of Izumi and Ikeda (2000). Single-crystal X-ray results for piemontite (Dollase 1969), parawollastonite (Trojer 1968), and bixbyite (Geller 1971) were used as initial parameters for the Rietveld refinement. The cell parameters determined using a unit-cell parameter refinement program in the RIGAKU RINT system were used as initial values. Peaks were defined using a "Modified split pseudo-Voigt" function, which comprised the split pseudo-Voigt function of Toraya (1990) combined with profile relaxation or the Pearson VII function in RIETAN-2000. An asymmetric parameter is built into this profile function. Details of these profile functions are given by Izumi and Ikeda (2000). Nonlinear least-squares calculation using the Marquardt method was followed by the conjugate-direction method to check convergence at local minima (Izumi 1993). Preferred orientation was corrected using the March-Dollase function (Dollase 1986).

Results

Synthesis experiments

Experimental conditions and the results of synthesis experiments are listed in Table 1. Results are arranged in order of ascending Mn^{3+} content in the starting material, $Ca_2Al_{3-q}Mn^{3+}_qSi_3O_{12.5}$ + H_2O, from q = 0.5 to 1.75 through 0.75, 1.0, 1.1, and 1.5.

The products from q = 0.5 starting material at 200 MPa and 500 °C (PM60) consisted mainly of piemontite, along with small amounts of associated anorthite. Although the anorthite content decreased with increasing duration, it persisted in the product with experiments up to 75 days in length. Contrary to this, in the synthesis experiments at 350 MPa with durations of 40 and 49 days, single-phase piemontite was successfully crystallized (PM46, PM27). Piemontite also crystallized as a single phase in the products from q = 0.75, 1.0, and 1.1 starting materials at pressures of 200 and 350 MPa and temperature of 500 °C.

The products from the q = 1.5 and 1.75 starting materials at pressures of 200 and 350 MPa consisted of a large amount of piemontite and a small amount of bixbyite ± trace parawollastonite. The amounts of bixbyite were distinctly greater than those of the products from starting materials with q less than 1.5. In the experiments using the q = 1.5 starting material at 200 MPa, we tried to synthesize piemontite at 500 °C (PM19) and at 550 °C (PM11, PM12) to compare the associated phases at different temperatures. However, the results were virtually identical.

Description and chemical compositions of synthetic phases

The piemontites synthesized in this study are prismatic crystals, generally 10 to 20 µm in length and a few to 5 µm in width. However, the piemontite crystals produced from q = 0.5 and 1.75 starting materials could not be analyzed due to their very narrow widths and sporadic distribution of bixbyite among piemontite aggregates, respectively. The chemical compositions of the synthetic piemontites are given in Table 2, where total Mn is shown as Mn_2O_3. The trivalent oxidation state of manganese is evidenced by the mineral assemblage of the solid buffer after the experiments, and by crystallization of piemontite and bixbyite in the products. The measured L_β/L_α value for Mn in the PM41 piemontite was 0.55, the same as that for natural and synthetic piemontites reported by Kimura and Akasaka (1999), indicating trivalent Mn. As shown in Table 2, the Mn^{3+} content (apfu) of piemontite is hereafter represented by the p-value in the formula $Ca_2Al_{3-p}Mn^{3+}_pSi_3O_{12}(OH)$.

The piemontites crystallized from q = 0.75, 1.0, and 1.1 starting materials had almost the same composition as their respective starting material. The p-value of piemontite from the q = 1.5 starting material at 200 and 350 MPa and 500 ºC was 1.3(1) on average, suggesting that the maximum Mn^{3+} content of piemontite in this study is 1.3(1) apfu. Our synthetic piemontites contain 2.01–2.07 Ca and 2.97–3.05 Si apfu, indicating that the A1 and A2 sites are filled with Ca^{2+}, the octahedral sites with Mn^{3+} and Al^{3+}, and the tetrahedral sites with Si^{4+}.

Bixbyite occurs as rounded grains. A pure Mn_2O_3 composition

was confirmed by EPMA analysis of this mineral in the PM63 and PM65 products. The Ca:Si-ratio of parawollastonite was almost 1:1, although the narrowness of the crystals precluded accurate analysis.

Rietveld refinement

Fourteen products were used for the X-ray structure refinements (Table 1). Details of data collection for the Rietveld analyses, the refined mass fractions and unit-cell parameters of each phase, *R*-factors, goodness-of-fit ($S = R_{wp}/R_e$), and the Durbin-Watson *d* statistic are listed in Table 3. Because the samples contained silver metal that was dissolved from the inner capsule and precipitated in the products, Ag metal was added to the refinement to improve the fit. Although the refinement details for Ag metal are not shown in Table 3, the structural parameters (space group $Fm\bar{3}m$) were fixed to initial values, and the unit-cell parameter and mass fraction were then refined: the a = 4.083–4.084 Å; the mass fraction = 0.00–0.04. In the Rietveld refinements, bixbyite and parawollastonite were also included as additional phases for each product, to refine the mass fractions of each phase. The mass fractions of bixbyite and parawollastonite in the products from the q = 0.5, 0.75, 1.0, and 1.1 starting materials are almost nil. However, in the products from the q = 1.5 starting material, the mass fractions of bixbyite and parawollastonite are 0.04–0.05 and 0.04–0.06, respectively. These increase in the products from the q = 1.75 starting material (Table 3). These facts are consistent with the results of chemical analyses of the piemontites. Figure 1 shows the result of Rietveld refinement of the product from the q = 1.0 starting material at 350 MPa and 500 °C (PM41).

On the basis of the chemical compositions of our piemontites, the Ca occupancy at the A1 and A2 sites and the Si occupancy at the T sites were both fixed at 1.00. The occupancy factors for Al and Mn^{3+} at the octahedral sites were refined using the following constraints: $Mn_{M1} = 1.0 - Al_{M1}$, $Mn_{M2} = 1.0 - Al_{M2}$, $Mn_{M3} = Mn_{total} - Mn_{M1} - Mn_{M2}$ and $Al_{M3} = 1.0 - Mn_{M3}$, where Mn_{total} is the value determined by EPMA analysis.

Occupancies of the octahedral sites and atomic positions refined in this study are reported in Tables 4 and 5, respectively. Interatomic distances and selected bond angles following from these atomic positions are listed in Tables 6 and 7, respectively.

TABLE 1. Synthesis data for the $Ca_2Al_3Si_3O_{12}(OH)$-$Ca_2Mn^{3+}_3Si_3O_{12}(OH)$ join

No.	q^*	P_{fluid} (MPa)	T (°C)	Duration (days)	Results
PM60	0.5	200	500	75	Pm+An
PM46	0.5	350	500	40	Pm
PM27	0.5	350	500	49	Pm
PM49	0.75	200	500	53	Pm
PM45	0.75	350	500	21	Pm
PM15	1.0	200	500	25	Pm
PM41	1.0	350	500	21	Pm
PM74	1.1	200	500	47	Pm (+Bix)
PM81	1.1	350	500	21	Pm (+Bix)
PM11	1.5	200	550	22	Pm+Bix (+Wo)
PM12	1.5	200	550	21	Pm+Bix (+Wo)
PM19	1.5	200	500	14	Pm+Bix (+Wo)
PM65	1.5	350	500	68	Pm+Bix (+Wo)
PM70	1.5	350	500	42	Pm+Bix (+Wo)
PM32	1.75	200	500	54	Pm+Bix (+Wo)
PM63	1.75	350	500	63	Pm+Bix
PM64	1.75	350	500	64	Pm+Bix (+Wo)

* q: Mn^{3+} in $Ca_2Al_{3-q}Mn^{3+}_qSi_3O_{12.5}$-oxide mixture
Pm: piemontite; An: anorthite; Bix: bixbyite; Wo: parawollastonite

DISCUSSION

Solubility of the $Ca_2Mn^{3+}_3Si_3O_{12}(OH)$-component in piemontite

In our study, the Mn^{3+}-contents (p) of the piemontites increased with increasing q-value of the starting material, and reached 1.3(1) apfu. This correlation is consistent with the mass fractions of the synthetic phases. The mass fractions of bixbyite and parawollastonite are nil or nearly nil in the products from starting materials with q value's of 0.5, 0.75, 1.0, and 1.1, and increase rapidly in the products from starting materials with q > 1.1. Moreover, cell parameters of piemontite crystallized from the q = 1.75 starting material had almost the same cell parameters as that from the q = 1.5 starting material, thus suggesting that the samples have the same Mn content. Thus, we conclude that the maximum Mn^{3+} content in piemontite synthesized at 500 ºC and 200 and 350 MPa is about 1.3 apfu. This value is considerably less than the maximum Mn^{3+}-content (about 1.9 apfu) reported for piemontite synthesized at 1.5 GPa and 800 °C (Anastasiou

TABLE 2. Chemical compositions of synthetic piemontites*

q		0.75		1.0		1.1		1.5	
Synthesis	P (MPa)	200	350	200	350	200	350	200	350
	T (ºC)	500	500	500	500	500	500	500	500
		n = 5	n = 26	n = 13	n = 20	n = 24	n = 25	n = 11	n = 9
SiO_2		36.99(34)	37.82(67)	37.48(51)	36.80(40)	35.84(31)	36.18(71)	36.58(95)	35.83(74)
Al_2O_3		23.40(50)	23.83(91)	19.33(87)	20.52(86)	20.06(36)	20.35(92)	17.76(171)	17.09(36)
Mn_2O_3		12.05(62)	12.29(101)	16.80(109)	16.19(156)	16.40(68)	16.40(106)	20.36(172)	19.49(42)
CaO		23.27(53)	23.51(61)	23.70(46)	23.39(31)	23.35(33)	23.25(35)	23.06(48)	22.70(19)
Total		95.71	97.45	97.31	96.90	95.65	96.18	97.76	95.11
					Cations per 12.5 O atoms				
Si		3.00(2)	3.01(3)	3.05(3)	3.00(2)	2.97(2)	2.98(3)	3.00(7)	3.02(5)
Al		2.24(5)	2.24(7)	1.85(8)	1.97(8)	1.96(3)	1.97(8)	1.71(15)	1.70(4)
Mn		0.74(4)	0.75(7)	1.03(8)	1.00(10)	1.04(5)	1.03(8)	1.26(12)	1.25(6)
Ca		2.02(5)	2.01(6)	2.07(4)	2.04(3)	2.07(3)	2.05(3)	2.03(5)	2.05(2)
Total		8.00	8.01	8.00	8.01	8.04	8.03	8.00	8.02
p		0.74	0.75	1.03	1.00	1.04	1.03	1.26	1.25

Notes: q: Mn^{3+} in $Ca_2Al_{3-q}Mn^{3+}_qSi_3O_{12.5}$-starting material. p: Mn^{3+} in $Ca_2Al_{3-p}Mn^{3+}_pSi_3O_{12}(OH)$-piemontite.
* Numbers in parentheses represent the standard deviations.

and Langer 1977). This difference may indicate a temperature and/or pressure dependence of maximum Mn^{3+} solubility in $Ca_2Al_3Si_3O_{12}(OH)$–$Ca_2Mn^{3+}_3Si_3O_{12}(OH)$ piemontite.

The maximum Mn^{3+} and $Mn^{3+} + Fe^{3+}$ contents (apfu) reported in natural Ca-piemontite are 1.25 Mn^{3+} (Mottana and Griffin 1986) and 1.12 Mn^{3+} + 0.34 Fe^{3+} (Akasaka et al. 1988), respectively. This is consistent with the experimental results described above, if the genetic conditions of natural piemontite are taken into consideration. Some Sr-rich piemontites contain more Mn^{3+} than common Ca-piemontite, even if their genetic conditions are similar; see, for example, tweddillite (Sr-rich piemontite) from the Kalahari manganese field, South Africa (1.58 Mn^{3+} + 0.19 Fe^{3+} = 1.77; Armbruster et al. 2002) and from the Fukuyama manganiferous iron ore deposit, Tokoro, Hokkaido (1.53 Mn^{3+} + 0.21 Fe^{3+} = 1.74; Akasaka et al. 1987). Enami and Banno (2001) reported tweddillite containing 1.42 Mn^{3+} + 0.81 Fe^{3+} (= 2.23 apfu) from Sanbagawa metamorphic rocks formed at higher pressure and temperature. High Sr contents at the A2 site seem to promote incorporation of Mn^{3+} at the M1 site.

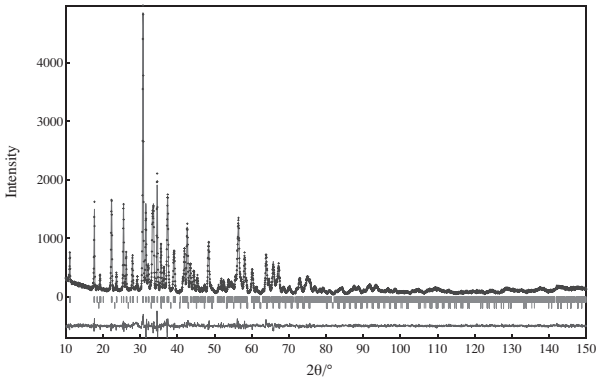

FIGURE 1. Rietveld refinement plot for the product (PM 41) from q = 1.0 starting material at 350 MPa and 500 °C. This product was refined with two phases (piemontite + bixbyite). The crosses are the observed data, the solid line is the calculated pattern, and the vertical bars mark all possible Bragg reflections (Cu$K\alpha_1$ and $K\alpha_2$). Upper and lower bar marks are piemontite and bixbyite, respectively. The difference between the observed and calculated patterns is shown at the bottom.

TABLE 3. Data collection* and details of structure refinement

q‡	0.5	0.75		1.0		1.1		1.5		1.75	
Synthesis P (MPa)	350	200	350	200	350	200	350	200	350	200	350
T (°C)	500	500	500	500	500	500	500	500	500	500	500
p‡	0.5†	0.75	0.75	1.00	1.00	1.04	1.03	1.26	1.25	1.26‡	1.25‡
Max. intensity (counts)	5631	5288	5544	4551	4973	5274	5028	4912	4854	2478	4769
					piemontite						
					$P2_1/m$						
a (Å)	8.856(1)	8.8530(5)	8.8548(8)	8.8531(8)	8.8490(9)	8.8596(5)	8.860(1)	8.8589(7)	8.8625(7)	8.8591(6)	8.8581(7)
b (Å)	5.6291(7)	5.6596(2)	5.6541(9)	5.6741(4)	5.6670(4)	5.6834(2)	5.6818(7)	5.7017(3)	5.7006(3)	5.7039(3)	5.6949(3)
c (Å)	10.148(1)	10.151(6)	10.1546(9)	10.1613(9)	10.153(1)	10.1679(6)	10.167(2)	10.1802(9)	10.1822(9)	10.1827(9)	10.1771(9)
β (°)	115.516(6)	115.511(4)	115.514(6)	115.519(6)	115.499(6)	115.503(4)	115.511(9)	115.540(6)	115.525(6)	115.548(6)	115.518(6)
V (Å^3)	456.58(9)	458.99(4)	458.82(7)	460.67(7)	459.75(7)	462.10(4)	461.9(1)	463.96(6)	464.21(6)	464.23(6)	463.31(6)
Z	2	2	2	2	2	2	2	2	2	2	2
R_B (%)§	1.57	2.12	1.75	2.14	2.11	2.07	1.87	3.15	3.43	2.66	3.37
R_F (%)§	0.91	0.99	0.85	1.23	1.04	1.23	0.90	2.13	2.14	2.10	1.91
R_p (%)§	7.62	7.49	6.58	8.37	7.11	7.46	7.50	7.27	7.71	8.69	7.27
R_{wp} (%)§	10.45	9.68	8.74	10.89	9.28	9.66	9.71	9.59	10.04	11.41	9.87
R_e (%)§	5.76	7.15	6.68	6.68	7.18	7.18	7.13	6.46	6.59	9.12	6.54
S§	1.812	1.353	1.308	1.630	1.291	1.346	1.362	1.484	1.523	1.251	1.511
D-W d‖	0.753	1.198	1.296	0.882	1.295	1.213	1.175	0.987	0.983	1.448	1.004
Mass fraction#											
Pm	0.987	0.989	0.960	0.982	0.993	0.983	0.981	0.912	0.900	0.874	0.824
Wo	0.013	0.011	0.032	0.010	0.000	0.000	0.000	0.044	0.043	0.050	0.089
Bix	0.000	0.000	0.008	0.008	0.007	0.017	0.019	0.044	0.057	0.076	0.087

* Step interval (°2θ) 10–150°, step 0.04°.
‡ Abbreviations as in Table 2.
† The p-value was fixed to the q-value of the starting material.
‡ Assumed to be the same as those of piemontites synthesized from q = 1.5 starting material at 200 and 350 MPa, respectively.
§ R_B:R-Bragg factor, R_F:R-structure factor, R_p:R-pattern, R_{wp}:R-weighted pattern, R_e:R-expected, S(=R_{wp}/R_e):Goodness of fit (Young 1993).
‖ D-W d: Durbin-Watson d-statistic (Hill and Flack 1987).
Abbreviations as in Table 1.

TABLE 4. Cation occupancies of the M1, M2, and M3 sites in synthetic piemontites, $Ca_2Al_{3-p}Mn^{3+}_pSi_3O_{12}(OH)$

q*		0.5	0.75		1.0	
Synthesis	P (MPa)	350	200	350	200	350
	T (°C)	500	500	500	500	500
p*		0.5†	0.75	0.75	1.00	1.00
M1		Al0.99(2)Mn0.01(2)	Al0.92(1)Mn0.08(2)	Al0.87(1)Mn0.13(2)	Al0.86(2)Mn0.14(2)	Al0.80(1)Mn0.20(1)
M2		Al0.96(2)Mn0.04(2)	Al0.98(1)Mn0.02(1)	Al0.97(2)Mn0.03(2)	Al0.95(2)Mn0.05(2)	Al1.00(1)Mn0.00(1)
M3		Al0.55(2)Mn0.45(2)	Al0.35(1)Mn0.65(2)	Al0.42(2)Mn0.58(2)	Al0.19(2)Mn0.81(2)	Al0.20(1)Mn0.80(1)

TABLE 5. Refined atomic positions of $Ca_2Al_{3-p}Mn^{3+}_pSi_3O_{12}(OH)$-piemontite

*q**				0.5	0.75		1.0		1.1		1.5		1.75	
Atom	neq†	W‡	x,y,z	350 MPa 500 °C	200 MPa 500 °C	350 MPa 500 °C	200 MPa 500 °C	350 MPa 500 °C	200 MPa 500 °C	350 MPa 500 °C	200 MPa 500 °C	350 MPa 500 °C	200 MPa 500 °C	350 MPa 500 °C
*p**				0.5	0.75	0.75	1.00	1.00	1.04	1.03	1.26	1.25	1.26	1.25
O1	4	f	x	0.232(2)	0.235(1)	0.231(1)	0.236(2)	0.233(1)	0.237(1)	0.238(1)	0.237(2)	0.238(2)	0.236(2)	0.241(2)
			y	0.991(2)	0.989(2)	0.990(2)	0.982(2)	0.986(2)	0.984(2)	0.986(2)	0.982(2)	0.980(2)	0.979(2)	0.985(2)
			z	0.036(1)	0.034(1)	0.034(1)	0.033(2)	0.030(1)	0.031(1)	0.031(1)	0.028(2)	0.029(2)	0.030(2)	0.030(2)
O2	4	f	x	0.301(1)	0.305(1)	0.308(1)	0.310(2)	0.308(1)	0.311(1)	0.310(1)	0.313(2)	0.312(2)	0.313(2)	0.311(2)
			y	0.986(2)	0.980(2)	0.979(2)	0.974(2)	0.975(2)	0.981(2)	0.981(2)	0.978(2)	0.978(2)	0.973(2)	0.981(2)
			z	0.358(2)	0.355(1)	0.358(1)	0.359(2)	0.353(1)	0.355(1)	0.358(1)	0.352(2)	0.350(2)	0.356(2)	0.353(2)
O3	4	f	x	0.789(1)	0.794(1)	0.794(1)	0.794(2)	0.795(1)	0.793(1)	0.792(2)	0.795(2)	0.796(2)	0.794(2)	0.802(2)
			y	0.013(2)	0.017(2)	0.017(2)	0.018(3)	0.019(2)	0.017(2)	0.022(2)	0.019(3)	0.017(3)	0.019(3)	0.015(3)
			z	0.352(1)	0.343(1)	0.342(1)	0.336(2)	0.338(1)	0.336(1)	0.335(1)	0.334(2)	0.333(2)	0.332(2)	0.337(2)
O4	2	e	x	0.065(2)	0.064(2)	0.059(2)	0.061(2)	0.064(2)	0.062(2)	0.063(2)	0.062(2)	0.067(2)	0.069(2)	0.068(2)
			y	1/4	1/4	1/4	1/4	1/4	1/4	1/4	1/4	1/4	1/4	1/4
			z	0.135(2)	0.132(2)	0.133(2)	0.133(2)	0.136(2)	0.134(2)	0.131(2)	0.140(2)	0.142(2)	0.135(3)	0.133(3)
O5	2	e	x	0.042(2)	0.042(2)	0.044(2)	0.038(2)	0.043(2)	0.043(2)	0.046(2)	0.044(2)	0.039(2)	0.038(2)	0.039(2)
			y	3/4	3/4	3/4	3/4	3/4	3/4	3/4	3/4	3/4	3/4	3/4
			z	0.147(2)	0.148(2)	0.149(2)	0.151(2)	0.147(2)	0.148(2)	0.151(2)	0.151(2)	0.154(2)	0.147(3)	0.150(2)
O6	2	e	x	0.063(2)	0.068(2)	0.065(2)	0.070(2)	0.066(2)	0.070(2)	0.070(2)	0.077(2)	0.079(2)	0.078(2)	0.078(2)
			y	3/4	3/4	3/4	3/4	3/4	3/4	3/4	3/4	3/4	3/4	3/4
			z	0.399(2)	0.406(2)	0.405(2)	0.407(3)	0.407(2)	0.413(2)	0.411(2)	0.414(2)	0.420(2)	0.417(3)	0.424(2)
O7	2	e	x	0.521(2)	0.517(2)	0.515(2)	0.519(2)	0.514(2)	0.512(2)	0.511(2)	0.514(2)	0.515(2)	0.528(2)	0.521(2)
			y	3/4	3/4	3/4	3/4	3/4	3/4	3/4	3/4	3/4	3/4	3/4
			z	0.181(2)	0.181(2)	0.173(2)	0.189(2)	0.181(2)	0.180(2)	0.182(2)	0.185(2)	0.184(2)	0.188(3)	0.184(2)
O8	2	e	x	0.521(2)	0.522(2)	0.520(2)	0.526(2)	0.524(2)	0.524(2)	0.523(2)	0.530(2)	0.531(3)	0.533(2)	0.531(3)
			y	1/4	1/4	1/4	1/4	1/4	1/4	1/4	1/4	1/4	1/4	1/4
			z	0.303(2)	0.309(1)	0.302(2)	0.308(2)	0.310(2)	0.310(2)	0.306(2)	0.312(2)	0.308(2)	0.309(3)	0.310(2)
O9	2	e	x	0.632(2)	0.621(2)	0.619(2)	0.615(2)	0.617(2)	0.614(2)	0.610(2)	0.606(2)	0.610(2)	0.612(2)	0.607(2)
			y	1/4	1/4	1/4	1/4	1/4	1/4	1/4	1/4	1/4	1/4	1/4
			z	0.095(2)	0.095(2)	0.097(2)	0.097(2)	0.094(2)	0.093(2)	0.090(2)	0.091(2)	0.088(2)	0.095(3)	0.085(2)
O10	2	e	x	0.075(2)	0.080(2)	0.089(2)	0.081(2)	0.080(2)	0.086(2)	0.086(2)	0.085(2)	0.088(2)	0.083(2)	0.085(2)
			y	1/4	1/4	1/4	1/4	1/4	1/4	1/4	1/4	1/4	1/4	1/4
			z	0.424(2)	0.424(1)	0.426(2)	0.420(2)	0.424(2)	0.424(2)	0.420(2)	0.421(2)	0.418(2)	0.415(2)	0.421(2)
Ca1	2	e	x	0.757(1)	0.756(1)	0.756(1)	0.756(1)	0.756(1)	0.757(1)	0.757(1)	0.756(1)	0.756(1)	0.756(1)	0.757(1)
			y	3/4	3/4	3/4	3/4	3/4	3/4	3/4	3/4	3/4	3/4	3/4
			z	0.155(1)	0.153(1)	0.154(1)	0.156(1)	0.152(1)	0.152(1)	0.152(1)	0.152(1)	0.151(1)	0.154(1)	0.154(1)
Ca2	2	e	x	0.603(1)	0.603(1)	0.600(1)	0.601(1)	0.599(1)	0.596(1)	0.598(1)	0.595(1)	0.594(1)	0.596(1)	0.594(1)
			y	3/4	3/4	3/4	3/4	3/4	3/4	3/4	3/4	3/4	3/4	3/4
			z	0.421(1)	0.424(1)	0.424(1)	0.424(1)	0.424(1)	0.423(1)	0.424(1)	0.421(1)	0.420(1)	0.423(1)	0.422(1)
M1	2	a	x	0	0	0	0	0	0	0	0	0	0	0
			y	0	0	0	0	0	0	0	0	0	0	0
			z	0	0	0	0	0	0	0	0	0	0	0
M2	2	c	x	0	0	0	0	0	0	0	0	0	0	0
			y	0	0	0	0	0	0	0	0	0	0	0
			z	1/2	1/2	1/2	1/2	1/2	1/2	1/2	1/2	1/2	1/2	1/2
M3	2	e	x	0.298(1)	0.295(1)	0.298(1)	0.300(1)	0.297(1)	0.300(1)	0.299(1)	0.304(1)	0.306(1)	0.301(1)	0.300(1)
			y	1/4	1/4	1/4	1/4	1/4	1/4	1/4	1/4	1/4	1/4	1/4
			z	0.222(1)	0.223(1)	0.222(1)	0.221(1)	0.222(1)	0.221(1)	0.222(1)	0.222(1)	0.222(1)	0.224(1)	0.222(1)
Si1	2	e	x	0.332(1)	0.337(1)	0.337(1)	0.335(1)	0.335(1)	0.335(1)	0.334(1)	0.338(1)	0.333(1)	0.338(1)	0.335(1)
			y	3/4	3/4	3/4	3/4	3/4	3/4	3/4	3/4	3/4	3/4	3/4
			z	0.046(1)	0.045(1)	0.045(1)	0.046(1)	0.043(1)	0.043(1)	0.042(1)	0.040(1)	0.040(1)	0.041(1)	0.043(1)
Si2	2	e	x	0.682(1)	0.681(1)	0.685(1)	0.687(1)	0.685(1)	0.688(1)	0.686(1)	0.687(1)	0.690(1)	0.686(1)	0.686(1)
			y	1/4	1/4	1/4	1/4	1/4	1/4	1/4	1/4	1/4	1/4	1/4
			z	0.275(1)	0.275(1)	0.275(1)	0.274(1)	0.274(1)	0.274(1)	0.274(1)	0.272(1)	0.271(1)	0.276(1)	0.271(1)
Si3	2	e	x	0.186(1)	0.186(1)	0.188(1)	0.184(1)	0.187(1)	0.187(1)	0.188(1)	0.186(1)	0.184(1)	0.186(1)	0.181(1)
			y	3/4	3/4	3/4	3/4	3/4	3/4	3/4	3/4	3/4	3/4	3/4
			z	0.317(1)	0.320(1)	0.319(1)	0.321(1)	0.318(1)	0.321(1)	0.320(1)	0.320(1)	0.321(1)	0.321(2)	0.322(1)

* Abbreviations as in Table 2.
† Multiplicity.
‡ Wyckoff letter.

TABLE 4—*continued*

*q**		1.1		1.5		1.75	
Synthesis	*P* (MPa)	200	350	200	350	200	350
	T (°C)	500	500	500	500	500	500
*p**		1.04	1.03	1.26	1.25	1.26‡	1.25‡
M1		Al0.84(1)Mn0.16(1)	Al0.81(1)Mn0.19(1)	Al0.73(1)Mn0.27(1)	Al0.68(1)Mn0.32(1)	Al0.69(2)Mn0.31(2)	Al0.73(2)Mn0.27(2)
M2		Al0.95(1)Mn0.05(1)	Al0.99(1)Mn0.01(1)	Al0.95(2)Mn0.05(2)	Al0.95(2)Mn0.05(2)	Al0.98(2)Mn0.02(2)	Al0.97(2)Mn0.03(2)
M3		Al0.17(1)Mn0.83(1)	Al0.17(1)Mn0.83(1)	Al0.06(2)Mn0.94(2)	Al0.11(2)Mn0.89(2)	Al0.08(2)Mn0.92(2)	Al0.05(2)Mn0.95(2)

* Abbreviations as in Table 2.
† The *p*-value was fixed to the *q*-value of the starting material.
‡ Assumed to be the same as those of piemontites synthesized from $q = 1.5$ starting material at 200 and 350 MPa, respectively.

TABLE 6. Interatomic distances (Å)

*q**		0.5	0.75		1.0		1.1		1.5		1.75		Dollase
Synthesis *P* (MPa)		350	200	350	200	350	200	350	200	350	200	350	(1969)
T (°C)		500	500	500	500	500	500	500	500	500	500	500	
*p**		0.5	0.75	0.75	1.00	1.00	1.04	1.03	1.26	1.25	1.26	1.25	
Ca1-O1	×2	2.46(1)	2.44(1)	2.45(1)	2.47(2)	2.41(1)	2.42(1)	2.41(1)	2.41(2)	2.41(2)	2.46(2)	2.41(2)	2.456(5)
-O3	×2	2.41(1)	2.35(1)	2.34(1)	2.30(2)	2.34(1)	2.32(1)	2.33(1)	2.32(2)	2.31(2)	2.29(2)	2.29(2)	2.324(5)
-O5		2.56(2)	2.56(1)	2.57(1)	2.51(2)	2.55(1)	2.55(1)	2.57(1)	2.55(2)	2.50(2)	2.52(2)	2.52(2)	2.557(6)
-O6		2.78(2)	2.85(1)	2.83(2)	2.85(2)	2.84(1)	2.90(1)	2.88(2)	2.94(2)	2.99(2)	2.95(2)	2.98(2)	2.873(6)
-O7		2.22(2)	2.25(1)	2.22(2)	2.27(2)	2.28(1)	2.30(1)	2.32(2)	2.31(2)	2.30(2)	2.20(2)	2.24(2)	2.288(6)
Average		2.47	2.46	2.46	2.45	2.45	2.46	2.46	2.47	2.46	2.45	2.45	2.468
-O9	×2	2.99(1)	3.03(1)	3.03(1)	3.05(1)	3.05(1)	3.06(1)	3.08(1)	3.09(1)	3.08(1)	3.08(1)	3.08(1)	3.05
Average		2.59	2.59	2.58	2.59	2.59	2.59	2.60	2.60	2.60	2.59	2.59	2.598
Ca2-O2	×2	2.81(1)	2.75(1)	2.71(1)	2.69(1)	2.68(1)	2.67(1)	2.68(1)	2.63(1)	2.63(2)	2.63(1)	2.65(2)	2.711(4)
-O2′	×2	2.51(2)	2.54(1)	2.53(1)	2.54(2)	2.58(1)	2.55(1)	2.52(1)	2.60(2)	2.62(1)	2.58(2)	2.58(2)	2.548(4)
-O3	×2	2.53(2)	2.65(1)	2.67(1)	2.71(2)	2.71(1)	2.73(1)	2.74(1)	2.76(1)	2.77(2)	2.78(2)	2.79(2)	2.745(4)
-O7		2.22(2)	2.25(1)	2.32(1)	2.18(2)	2.25(2)	2.26(1)	2.24(2)	2.19(2)	2.20(2)	2.20(2)	2.22(2)	2.277(6)
-O10		2.59(1)	2.56(1)	2.51(2)	2.57(2)	2.58(1)	2.56(1)	2.55(1)	2.58(2)	2.59(2)	2.60(2)	2.60(2)	2.541(7)
Average		2.56	2.59	2.58	2.58	2.60	2.59	2.58	2.59	2.60	2.60	2.61	2.603
-O8	×2	3.02(1)	3.03(1)	3.04(1)	3.03(1)	3.02(1)	3.03(1)	3.04(1)	3.02(1)	3.03(1)	3.04(1)	3.03(1)	3.03
Average		2.66	2.68	2.67	2.67	2.68	2.68	2.68	2.68	2.69	2.69	2.69	2.689
Si1-O1	×2	1.59(2)	1.60(1)	1.63(1)	1.56(1)	1.59(1)	1.57(1)	1.56(1)	1.57(1)	1.53(1)	1.56(1)	1.55(1)	1.654(5)
-O7		1.65(2)	1.60(1)	1.55(1)	1.66(2)	1.60(1)	1.59(1)	1.60(2)	1.62(2)	1.64(2)	1.71(2)	1.65(2)	1.569(7)
-O9		1.59(2)	1.62(2)	1.64(2)	1.67(2)	1.62(1)	1.63(1)	1.63(2)	1.62(2)	1.59(2)	1.62(2)	1.58(2)	1.638(7)
Average		1.61	1.61	1.61	1.61	1.60	1.59	1.59	1.60	1.57	1.61	1.58	1.629
Si2-O3	×2	1.63(1)	1.62(1)	1.60(1)	1.58(1)	1.59(1)	1.59(1)	1.57(1)	1.59(1)	1.59(1)	1.58(2)	1.65(2)	1.619(5)
-O8		1.58(2)	1.58(2)	1.59(2)	1.61(2)	1.61(2)	1.65(2)	1.61(2)	1.61(2)	1.61(2)	1.53(2)	1.58(2)	1.608(7)
-O9		1.68(2)	1.67(1)	1.65(2)	1.63(2)	1.66(2)	1.66(1)	1.69(2)	1.67(2)	1.69(2)	1.67(2)	1.72(2)	1.634(7)
Average		1.63	1.62	1.61	1.60	1.61	1.62	1.61	1.62	1.62	1.59	1.65	1.620
Si3-O2	×2	1.61(1)	1.61(1)	1.61(1)	1.62(1)	1.61(1)	1.65(1)	1.64(1)	1.66(1)	1.66(1)	1.63(1)	1.69(1)	1.627(5)
-O5		1.65(2)	1.66(1)	1.65(2)	1.66(2)	1.65(2)	1.67(2)	1.63(2)	1.64(2)	1.63(2)	1.69(2)	1.66(2)	1.671(7)
-O6		1.64(2)	1.63(2)	1.67(2)	1.60(2)	1.67(2)	1.66(2)	1.66(2)	1.62(2)	1.64(2)	1.64(3)	1.65(2)	1.649(7)
Average		1.63	1.63	1.64	1.63	1.64	1.66	1.64	1.65	1.65	1.65	1.67	1.644
M1-O1	×2	1.92(1)	1.96(1)	1.92(1)	1.97(1)	1.95(1)	1.99(1)	2.00(1)	1.99(1)	2.01(2)	1.98(1)	2.02(2)	1.941(4)
-O4	×2	1.87(1)	1.86(1)	1.87(1)	1.87(1)	1.89(1)	1.88(1)	1.86(1)	1.92(1)	1.93(2)	1.89(2)	1.88(2)	1.872(5)
-O5	×2	1.97(2)	1.98(1)	1.98(1)	2.01(2)	1.98(1)	1.99(1)	2.00(1)	2.01(1)	2.03(2)	1.99(2)	2.01(2)	1.985(5)
Average		1.92	1.93	1.92	1.95	1.94	1.95	1.95	1.97	1.99	1.95	1.97	1.933
M2-O3	×2	1.82(1)	1.84(1)	1.84(1)	1.87(1)	1.85(1)	1.88(1)	1.89(1)	1.88(1)	1.88(2)	1.89(2)	1.83(2)	1.857(4)
-O6	×2	1.96(2)	1.94(1)	1.93(1)	1.94(2)	1.92(1)	1.92(1)	1.93(1)	1.94(2)	1.92(2)	1.93(2)	1.89(2)	1.934(5)
-O10	×2	1.86(2)	1.89(1)	1.92(1)	1.92(2)	1.89(1)	1.92(1)	1.95(1)	1.94(2)	1.97(1)	1.97(2)	1.94(2)	1.881(6)
Average		1.88	1.89	1.90	1.91	1.89	1.91	1.92	1.92	1.92	1.93	1.89	1.891
M3-O1	×2	2.25(1)	2.30(1)	2.27(1)	2.31(1)	2.33(1)	2.32(1)	2.33(1)	2.36(1)	2.36(1)	2.38(2)	2.35(1)	2.274(5)
-O2	×2	2.02(1)	2.01(1)	2.04(1)	2.08(2)	2.02(1)	2.02(1)	2.04(1)	2.02(1)	2.01(1)	2.04(2)	2.00(2)	2.031(5)
-O4		1.86(2)	1.84(1)	1.91(1)	1.91(2)	1.86(1)	1.90(1)	1.89(1)	1.93(2)	1.91(2)	1.86(2)	1.86(2)	1.900(6)
-O8		1.78(2)	1.82(1)	1.78(2)	1.80(2)	1.81(1)	1.79(1)	1.79(2)	1.81(2)	1.80(2)	1.86(2)	1.84(2)	1.861(6)
Average		2.03	2.05	2.05	2.08	2.06	2.06	2.07	2.08	2.09	2.09	2.07	2.062

* Abbreviations as in Table 2.

TABLE 7. Selected interatomic angles (°)

*q**		0.5	0.75		1.0		1.1		1.5		1.75	
Synthesis *P* (MPa)		350	200	350	200	350	200	350	200	350	200	350
T (°C)		500	500	500	500	500	500	500	500	500	500	500
*p**		0.5	0.75	0.75	1.00	1.00	1.04	1.03	1.26	1.25	1.26	1.25
O1-Si1-O1′		116.0(11)	115.1(9)	113.0(10)	115.5(14)	115.2(10)	116.3(10)	118.0(11)	114.8(13)	117.1(15)	113.3(14)	119.4(13)
O1-Si1-O7		112.8(6)	112.4(5)	113.9(6)	111.8(7)	112.8(5)	112.0(6)	111.0(6)	111.5(8)	111.2(8)	112.5(8)	111.8(8)
O1-Si1-O9		105.4(6)	106.0(4)	106.8(6)	106.4(7)	106.2(5)	106.5(5)	106.8(6)	107.5(7)	107.4(7)	107.5(8)	105.9(7)
O7-Si1-O9		103.0(10)	103.8(7)	101.4(9)	103.8(11)	102.4(8)	102.3(8)	101.7(9)	103.3(10)	101.3(11)	102.7(11)	99.7(11)
O3-Si2-O3′		110.1(11)	109.0(8)	110.8(10)	112.2(13)	110.4(9)	113.2(10)	111.8(11)	112.1(12)	113.2(14)	112.5(13)	109.1(12)
O3-Si2-O8		107.2(7)	111.0(5)	111.0(6)	110.5(8)	110.5(6)	109.4(6)	111.0(7)	109.9(8)	109.4(9)	112.0(9)	111.0(8)
O3-Si2-O9		110.5(7)	107.9(5)	109.1(6)	108.8(8)	108.6(6)	109.1(5)	108.8(6)	109.5(8)	109.6(7)	106.8(8)	109.0(7)
O8-Si2-O9		111.2(10)	110.0(8)	105.6(9)	105.9(12)	108.2(8)	106.3(9)	105.1(9)	105.8(11)	105.2(12)	106.3(13)	107.8(11)
O2-Si3-O2′		111.0(10)	107.7(8)	107.2(10)	103.0(11)	104.9(8)	105.6(9)	106.2(9)	103.0(10)	102.4(11)	102.7(11)	102.5(11)
O2-Si3-O5		112.7(7)	111.5(5)	112.8(6)	113.5(9)	111.7(6)	111.0(6)	112.4(7)	110.8(8)	110.9(8)	112.2(10)	110.2(9)
O2-Si3-O6		110.7(8)	112.7(5)	112.3(7)	100.4(10)	114.1(6)	113.6(6)	101.4(9)	114.4(8)	114.6(8)	113.3(9)	113.6(9)
O5-Si3-O6		98.4(9)	100.7(7)	99.4(8)	100.4(10)	100.6(8)	102.3(8)	101.4(9)	103.7(9)	103.7(10)	103.5(11)	106.7(10)
O1-M1-O4		85.1(6)	85.8(4)	86.8(5)	87.6(6)	87.1(4)	82.8(4)	87.1(5)	89.2(5)	88.1(6)	87.0(7)	86.2(7)
O1-M1-O5		90.0(5)	89.8(4)	90.1(5)	89.0(6)	89.6(4)	89.9(4)	90.0(5)	89.5(5)	88.4(6)	89.1(6)	88.1(6)
O4-M1-O5		94.8(6)	95.6(4)	95.1(5)	94.9(6)	94.9(5)	95.0(4)	95.2(5)	93.6(6)	92.6(6)	95.5(8)	95.3(7)
O3-M2-O6		91.1(6)	90.8(4)	90.1(5)	90.0(6)	89.8(5)	90.8(5)	90.9(5)	91.5(6)	92.1(7)	91.9(8)	92.2(7)
O3-M2-O10		87.1(6)	89.4(5)	87.8(5)	91.2(7)	90.5(5)	89.5(5)	90.7(5)	91.1(6)	91.2(7)	92.3(7)	91.0(7)
O6-M2-O10		95.5(7)	95.5(4)	94.6(5)	94.7(7)	96.2(4)	85.6(4)	94.3(5)	94.4(6)	94.3(6)	94.2(7)	96.3(7)
O1-M3-O1′		80.7(6)	80.2(5)	80.6(5)	82.2(7)	80.1(5)	81.2(5)	80.3(5)	80.8(7)	81.3(7)	81.3(7)	80.0(7)
O1-M3-O2		91.0(5)	89.8(3)	90.1(4)	89.3(5)	88.8(4)	89.6(4)	90.5(4)	88.6(5)	87.8(5)	88.2(5)	89.6(5)
O1-M3-O4		76.7(6)	77.2(4)	76.5(5)	77.5(6)	77.4(4)	78.2(5)	77.5(5)	78.8(6)	78.8(7)	77.0(8)	77.8(7)
O1-M3-O8		103.0(6)	102.0(4)	102.9(5)	103.2(6)	103.3(4)	103.7(4)	102.1(5)	104.4(5)	103.6(6)	102.0(6)	102.1(6)
O2-M3-O2′		94.6(8)	99.0(5)	97.2(7)	97.6(8)	101.0(6)	98.3(6)	97.5(7)	100.4(8)	101.1(8)	101.0(9)	99.5(8)
O2-M3-O4		90.4(6)	93.2(4)	91.9(5)	91.9(6)	92.3(4)	92.0(5)	92.9(5)	90.6(6)	89.6(6)	93.1(7)	92.8(7)
O2-M3-O8		89.8(5)	87.5(4)	88.6(5)	87.5(6)	87.0(4)	86.3(4)	87.4(4)	86.7(5)	88.3(6)	87.8(6)	87.3(6)
Si1-O9-Si2		155.8(11)	151.4(9)	149.0(10)	145.8(13)	147.0(9)	144.5(10)	142.9(11)	141.1(12)	140.7(14)	145.0(14)	142.9(13)

* Abbreviations as in Table 2.

Mn^{3+} occupancies of the M1, M2, and M3 sites

The distribution of the majority of Mn^{3+} at M3 and a little at M1 is well illustrated in Figure 2, where the refined Mn^{3+} occupancies of the M1, M2, and M3 sites are plotted as a function of the *p*-value of the synthetic $Ca_2Al_{3-p}Mn^{3+}_pSi_3O_{12}(OH)$-piemontites. Langer et al. (2002) produced a similar diagram using their results for three synthetic piemontites (1.5 GPa and 800 °C) and some natural piemontites. It is significant that the Mn^{3+} occupancies of the M1 and M3 sites in the synthetic piemontites refined by Langer et al. (2002) almost lie on the regression curves from our present study, indicating that the distribution of Mn^{3+} at the M3 and M1 sites is not influenced significantly by crystallization pressures and temperatures.

The relationship between the Mn^{3+} occupancy of the M3 site ($[g_{Mn^{3+}}]^{M3}$) and *p*-value can be approximated by the regression curve;

$$[g_{Mn^{3+}}]^{M3} = -0.20p^2 + 1.00p \ (R^2 = 0.98) \quad (1)$$

and the Mn^{3+} occupancy of the M1 site ($[g_{Mn^{3+}}]^{M1}$) vs. *p*-value by

$$[g_{Mn^{3+}}]^{M1} = 0.23p^2 - 0.06p \ (R^2 = 0.93) \quad (2)$$

Although the M2 site is occupied only by Al in the natural piemontites referred to above and in some synthetic piemontites (Langer et al. 2002), Mn^{3+} occupancies up to 0.05 apfu were refined at the M2 site in our results. Since these occupancies are generally less than the 2σ error, our result may not be direct evidence of the existence of Mn^{3+} at the M2 site. However, Giuli et al. (1999) reported that a little Fe^{3+} (up to 0.08 Fe^{3+} apfu) occupied the M2 site in synthetic epidotes crystallized at 700 °C and 460–530 MPa. Thus Mn^{3+} may enter the M2 site under any *P-T* conditions of piemontite crystallization.

The relationship of Mn^{3+} concentrations at the M1 and M3 sites are shown in Figure 3, using the intracrystalline partition coefficient K_D, which is defined as

$$K_D = (Mn^{3+}/Al) \text{ in M1}/(Mn^{3+}/Al) \text{ in M3}. \quad (3)$$

Most piemontites synthesized in the present study have K_D values between 0.038 and 0.063, whereas three synthetic piemontites studied by Langer et al. (2002) have K_D-values between 0.063 (Mn^{3+}_{M1}:Mn^{3+}_{M3} = 0.460:0.931) and 0.080 (Mn^{3+}_{M1}:Mn^{3+}_{M3} = 0.168:0.715). The K_D-values of Fe^{3+} [K_D = (Fe^{3+}/Al) in M1/(Fe^{3+}/Al) in M3] in synthetic and natural epidotes range from 0.01 to 0.025 (Dollase 1973) or 0.033 to 0.054 (Giuli et al. 1999). Thus, K_D-values of piemontite tend to be larger than those of epidote. This suggests that Fe^{3+} preference at the M3 site is stronger than Mn^{3+} preference, although the strong preference of Mn^{3+} for the M3 site has been explained in terms of the Jahn-Teller effect. Dollase (1973) also discussed this odd result, on the basis of his studies of Mn^{3+} and Fe^{3+}occupancies in St. Marcel piemontite. This problem requires further investigation.

Bond lengths and angles

Although the bond lengths and angles derived from our powder data (Tables 6 and 7) have larger standard deviations than those of single-crystal data from natural and synthetic piemontites, the values themselves are almost consistent with the published data. The mean Ca1-O, Ca2-O, Si1-O, Si2-O, and Si3-O bond distances are the same as those reported by Dollase

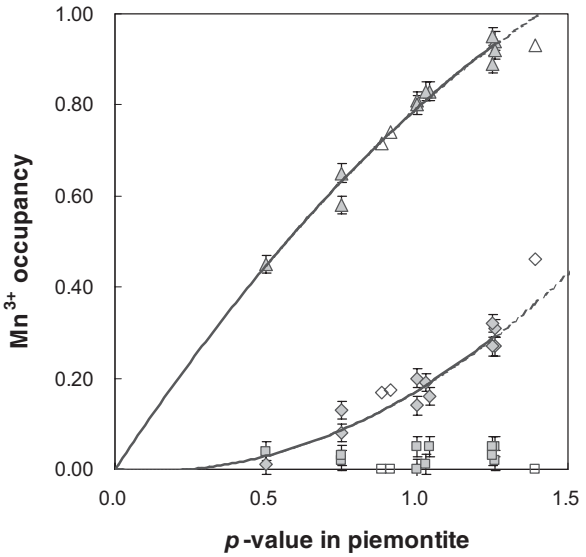

FIGURE 2. Variation of the Mn^{3+} occupancies of the M1, M2, and M3 sites in piemontite as a function of *p*-value. Closed triangles, closed diamonds, and closed squares represent Mn^{3+}-occupancies at the M3, M1, and M2 sites in this study, respectively. Open triangles, open diamonds, and open squares designate Mn^{3+} occupancies at the M3, M1, and M2 sites after Langer et al. (2002), respectively. Error bars represent 1σ standard deviation.

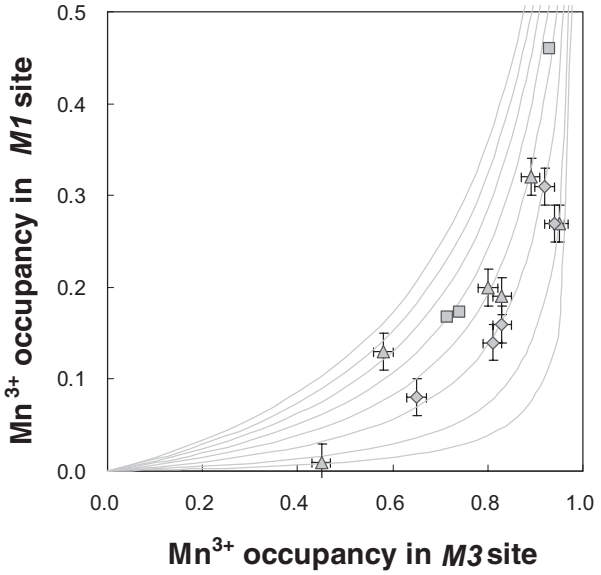

FIGURE 3. Mn^{3+} occupancy at the M1 site vs. Mn^{3+} occupancy at the M3 site [K_D = (Mn^{3+}/Al) in M1 / (Mn^{3+}/Al) in M3]. Ideal fractionation K_D values of 0.01, 0.02, 0.04, 0.06, 0.08, 0.10, 0.12, and 0.14 are shown. Closed diamonds and triangles denote synthetic piemontites at 200 MPa and 350 MPa in this study, respectively. Closed squares represent synthetic piemontites obtained by Langer et al. (2002).

(1969) within 1 or 2σ. The interatomic distances at the M1, M2, and M3 sites of $p = 1.0$ piemontite can be compared to that published by Langer et al. (2002) for synthetic piemontite with $p = 0.98$ (single-crystal data). Our results for $p = 1.0$ piemontite synthesized at 350 MPa are generally consistent with those of Langer et al. (2002) within 1 or 2σ. However, the powder data for the $p = 1.0$ piemontite at 200 MPa deviate somewhat from the single-crystal data of Langer et al. (2002). This deviation may be due to errors in the structural refinement of $p = 1.0$ piemontite at 200 MPa caused by serial correlation between adjacent points in diffraction patterns, as shown by the low Durbin-Watson *d*-statistic of 0.882 (Table 3).

For consideration of the variations of each M-O distances (Fig. 4), we used the published structural parameters of clinozoisite from Dollase (1968) as data at $p = 0$. The mean M1-O distance ranges between 1.92 and 1.99, and changes with increasing *p*-value in piemontite thus:

$$<\text{M1-O}>_{\text{mean}} (\text{Å}) = 0.05p^2 - 0.01p + 1.91 \ (R^2 = 0.78) \quad (4)$$

As shown in Figure 4, although the M1-O1, M1-O4, and M1-O5 bond lengths increase with increasing *p*-value, the changes in the M1-O1 distance is remarkable. The mean M3-O distance in piemontite changes from 2.03 to 2.09 Å with increasing *p*:

$$<\text{M3-O}>_{\text{mean}} (\text{Å}) = -0.03p^2 + 0.11p + 1.98 \ (R^2 = 0.77) \quad (5)$$

The change in $<\text{M3-O}>_{\text{mean}}$ is mainly caused by the variations of M3-O1 distance.

Although the bond distances show non-linear variation against *p*-values, a linear relationship exists between M3-O and M1-O distances and Mn^{3+} contents at the M3 and M1 sites, respectively, as shown in Figure 5. The progressive decrease of the Si1-O9-Si2 angle with increasing *p*-value in piemontite, which has previously been reported (e.g., Langer et al. 2002) was also confirmed in this study. We also found systematic variation of the O5-Si3-O6 angle with increasing *p*-value (Fig. 6):

$$\angle\text{O5-Si3-O6} = 8.33p^2 - 7.20p + 100.20 \ (R^2 = 0.81) \quad (6)$$

This relation implies that the O5-Si3-O6 angle is reduced with increasing *p*-value up to near 0.75, and then increases with increase of *p* above 0.75. As discussed later, this effects the change in the *c* dimension.

Relationship between unit-cell parameters and bond lengths and angles

Figure 7 shows the variations of the unit-cell parameters as a function of *p*-value for piemontite. The *a* parameter decreases with increasing *p* up to near 1, and increases with increasing *p* over about 1, whereas the *c* dimension does not change significantly from $p = 0.0$ to about $p = 0.75$, but increases steeply above $p = 0.75$. These variations are similar to those reported by Anastasiou and Langer (1977). However, our results do not necessarily support the interpretation by Anastasiou and Langer (1977) that these breaks in the unit-cell parameters are due to predominant entrance of Mn^{3+} into the M3 site below $p = 1.0$ and into M1 above $p = 1.0$. Firstly, in our study there seems not to be

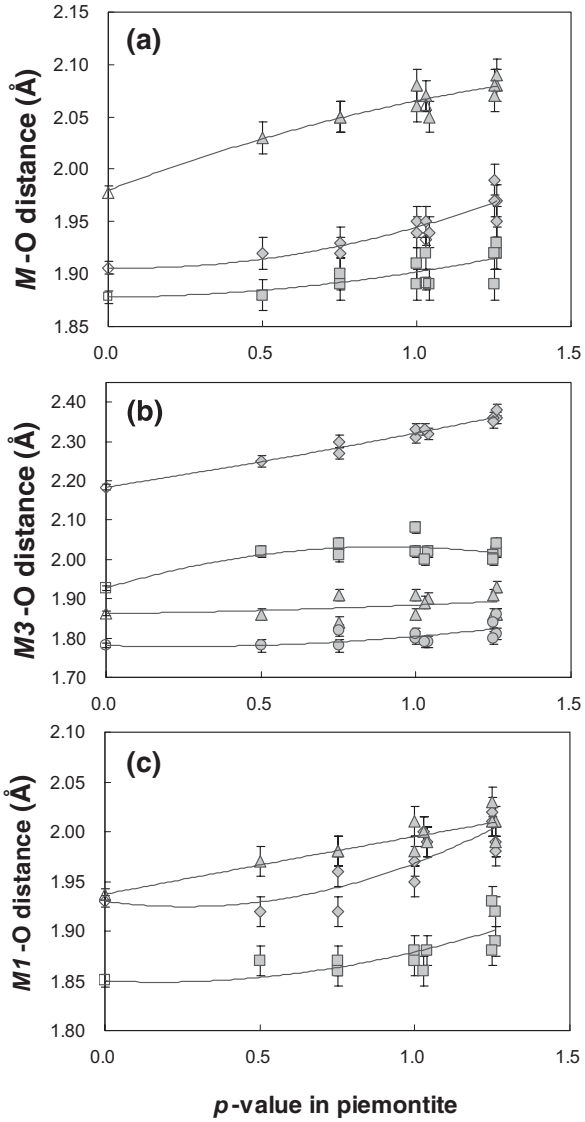

Figure 4. Variations of M-O distances as a function of *p*-value in piemontite. (**a**) Mean M-O distances. Closed diamonds represent M1 site (this study); closed squares M2 site (this study); closed triangles M3 sites (this study); open diamonds M1 sites (Dollase 1968, 1969); open squares M2 sites (Dollase 1968, 1969); open triangles M3 site (Dollase 1968, 1969). (**b**) M3-O*i* distances. Closed diamonds represent M3-O1 distances (this study); closed squares M3-O2 distances (this study); closed triangles M3-O4 distances (this study); closed circles M3-O8 distances (this study); open diamond M3-O1 distance (Dollase 1968); open square M3-O2 distance (Dollase 1968); open triangle M3-O4 distance (Dollase 1968); open circle M3-O8 distance (Dollase 1968). (**c**) M1-O*i* distances. Closed diamonds represent M1-O1 distances (this study); closed squares M1-O4 distances (this study); closed triangles M1-O5 distances (this study); open diamond represent M1-O1 distance (Dollase 1968); open square M1-O4 distance (Dollase 1968); open triangle M1-O5 distance (Dollase 1968).

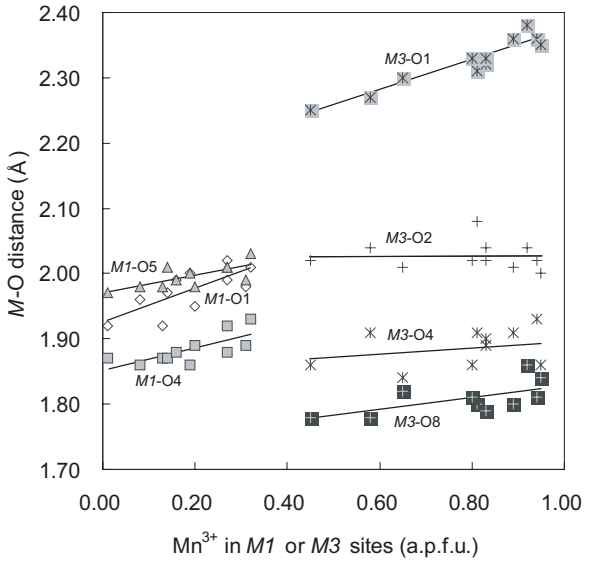

FIGURE 5. Variations of M-O distances as a function of Mn^{3+} content (apfu) at M1 or M3 sites.

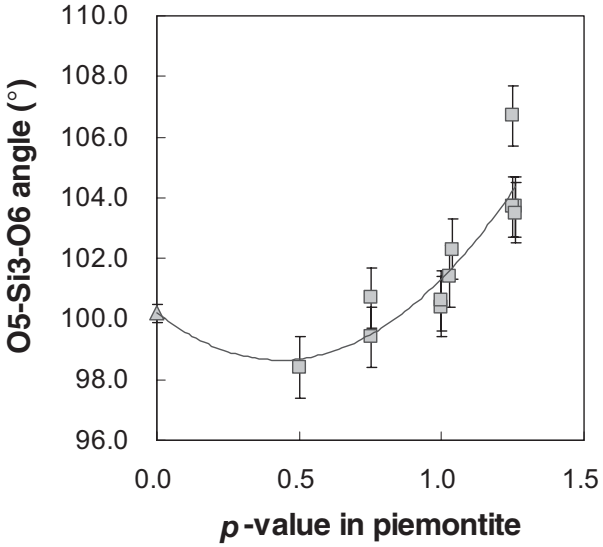

FIGURE 6. Variation of O5-Si3-O6 angle as a function of *p*-value in piemontite.

a break between each cell dimension near $p = 1$, and secondly, the interpretation of the "break" of cell parameters by Anastasiou and Langer (1977) does not seem reasonable, because Mn^{3+} enters the M1 site even if the M3 site is not filled by Mn^{3+}, and thus the change of the cell dimensions must be gradual. For example, we can formulate the variations of the cell volume by function of *p* value as follows: V (Å^3) = $3.74p^2 + 3.92p + 454.36$ ($R^2 = 0.95$), where we used the published cell parameters of clinozoisite by Dollase (1968) as the values at $p = 0$.

The variations of the *a* and *c* dimensions with *p* are similar to that of mean M1-O distance (Eq. 4), and the *b* dimension to that of mean M3-O distance (Eq. 5). However, the changes of

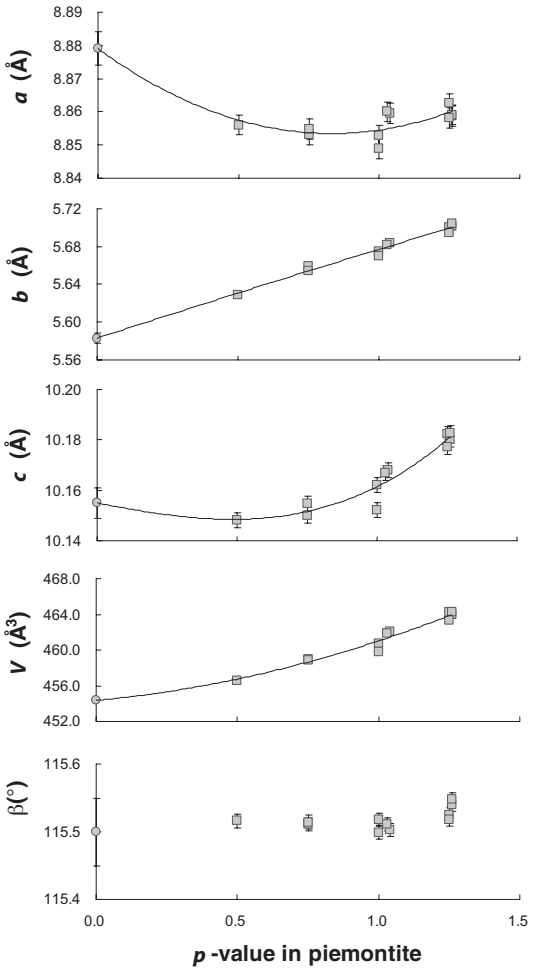

FIGURE 7. Variations of unit-cell parameters as a function of *p*-value in piemontite. Error bars represent 1σ standard deviation. Closed squares denote synthetic piemontites in this study (Table 3). Closed circle denotes clinozoisite data obtained by Dollase (1968).

mean M-O distances do not fully coincide with those of the *a* and *c* parameters. As shown in an **a**-**c** projection of the crystal structure of piemontite (Fig. 8), the *a* dimension depends mainly on the M1-O1 distance. On the basis of variation of each M-O bond length, we interpret that the nonlinear variation of the *a* dimension is caused by the change of M1-O1 distance with *p*. On the other hand, the *c* dimension might be strongly influenced by the M3-O1, M1-O4, and M1-O5 distances. However, the variation of the *c* parameter is not necessarily consistent with the changes of M3-O1, M1-O4, and M1-O5 distances. This problem is solved when we take into consideration the variation of the O5-Si3-O6 angle. This controls the O5-O6 distance (Eq. 6), which effects the *c* dimension. Since the increase of the M1-O5 distance and the shrinkage of the O5-O6 distance caused by reduction of the O5-Si3-O6 angle with the increase of *p* from 0 to 0.75 counteract each other, the *c* parameter scarcely changes. However, when the *p*-value is over 1.0, increase of the O5-Si3-O6 angle causes extension of the O5-O6 distance and elongation of the *c* dimension.

TABLE 8. Bond length and angular distortion of the octahedral sites in synthetic piemontites

*q**	0.5	0.75		1.0		1.1		1.5		1.75	
Synthesis *P* (MPa)	350	200	350	200	350	200	350	200	350	200	350
T (°C)	500	500	500	500	500	500	500	500	500	500	500
*p**	0.5	0.75	0.75	1.00	1.00	1.04	1.03	1.26	1.25	1.26	1.25
DI(oct)											
M1 site	0.017	0.025	0.020	0.027	0.017	0.025	0.032	0.018	0.020	0.022	0.031
M2 site	0.028	0.018	0.020	0.014	0.013	0.009	0.012	0.014	0.016	0.014	0.020
M3 site	0.072	0.083	0.071	0.073	0.087	0.084	0.084	0.089	0.092	0.091	0.091
$\sigma(oct)^2$											
M1 site	17.84	17.83	13.19	11.19	11.85	27.95	12.89	5.04	4.70	14.57	16.78
M2 site	14.50	11.36	9.46	8.56	14.08	7.36	7.20	8.30	8.85	9.65	16.56
M3 site	72.89	75.07	77.15	72.75	83.80	75.99	71.60	80.44	75.95	75.92	73.76

Notes: Bond length distortion parameter defined by Baur (1974): DI (oct) = $1/6\ \Sigma|R_i - R_{av}|/R_{av}$, where R_i is each bond length and R_{av} is the average distance for an octahedron. Angular distortion parameter defined by Robinson et al. (1971): $\sigma(oct)^2 = \Sigma(\theta_i - 90^o)/11$ (θ_i: O-M-O angle).
* Abbreviations as in Table 2.

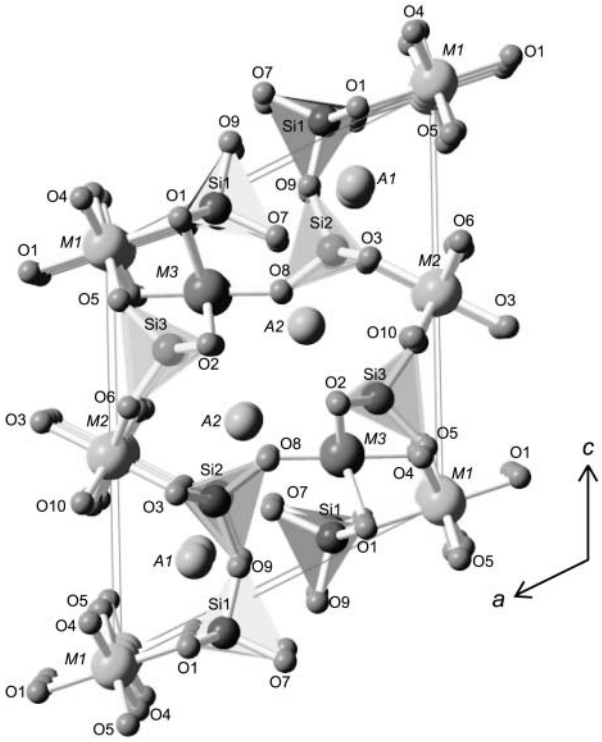

FIGURE 8. The **a-c** projection of the crystal structure of p = 1.0 piemontite.

Bond length and angular distortions of the octahedral sites

Deformation of the M1 and M3 octahedra of piemontite with incorporation of Mn^{3+} has been noted previously (Dollase 1969). However, Bermanec et al. (1994) observed that piemontites with high Mn^{3+} contents do not show stronger deformation due to Jahn-Teller distortion than do epidotes and clinozoisite, and Ferraris et al. (1989) considered that M-site distortions did not affect Fe and Mn occupancies of the M-sites.

To examine their results, we calculated bond length and angular distortion parameters defined by Baur (1974) and Robinson et al. (1971) as shown in Table 8. The values of the bond length distortion parameter of the M3 site (DI_{M3}) increases with increasing p-value. Angular distortion of the M3 site is greater than those of M1 and M2, and tends to increase with increasing p-value. These results are consistent with the greatest Mn^{3+} occupancy of the M3 site and the site distortions of that site by the Jahn-Teller effect. Langer et al. (2002) mentioned that increasing M3-O*i* distance causes increasing relative compression along O4-M3-O8 as Mn^{3+} at the M3 site increases. Our results indicate that, with increasing of $<M3\text{-}O>_{mean}$, deformation of the M3 octahedra to the tetragonally compressed octahedron is caused by extension of O1-M3-O2 relative to O4-M3-O8 with the increase in p-value.

In contrast to the M3 site, the variation of the bond length distortion and angular distortion of the M1 site is not clear. This may be due to more equidimensional expansion of the M1 octahedra against the Mn^{3+} content in the M1 site (Fig. 5) than the M3 octahedra.

Since the M3 octahedra are essentially larger and more distorted than M1 octahedra in epidote group minerals, Mn^{3+}-ions tend to occupy the M3 site, and the M3 site becomes more and more distorted with increasing Mn^{3+} at the site. Conversely, the M1 site is smaller and more regular in shape than the M3 site, and thus Mn^{3+}-preference of the M1 site is less than that of the M3 site. This interpretation seems to be reasonable for the explanation of Mn^{3+} distribution among the M1 and M3 sites, but it does not explain well the stronger preference of Fe^{3+} rather than Mn^{3+} for the M3 site. This problem is an interesting subject for future study.

ACKNOWLEDGMENTS

Our thanks to F. Izumi of the National Institute for his permission to use the Rietan-2000 program and for his help; to K. Makino of Shinshu University for helpful discussion on crystal structure analysis; and to B. Roser of Shimane University for his critical reading of the manuscript. We also thank P. Bonazzi and an anonymous referee for their valuable comments, and S. Quartieri for editorial assistance.

REFERENCES CITED

Akasaka, M., Sakakibara, M., and Togari, K. (1987) Sr-piemontite from manganiferous hematite ore deposit, Tokoro belt. Annual Meeting of Mineral Society Japan, p. 96.

——— (1988) Piemontite from the manganiferous hematite ore deposits in the Tokoro belt, Hokkaido, Japan. Mineralogy and Petrology, 38, 105–116.

Akasaka, M., Zheng, Y., and Suzuki, Y. (2000) Maximum strontium content of piemontite formed by hydrothermal synthesis. Journal of Mineralogical and Petrological Sciences, 95, 84–94.

Akasaka, M., Suzuki, Y., and Watanabe, H. (2003) Hydrothermal synthesis of pumpellyite-okhotskite series minerals. Mineralogy and Petrology, 77, 25–37.

Albee, A.L. and Chodos, A.A. (1970) Semiquantitative electron microprobe determination of Fe^{2+}/Fe^{3+} and petrologic problems. American Mineralogist, 55, 491–501.

Anastasiou, P. and Langer, K. (1977) Synthesis and physical properties of piemontite $Ca_2Al_{3-p}Mn^{3+}{}_p(Si_2O_7/SiO_4/O/OH)$. Contributions to Mineralogy and Petrology,

60, 225–245.
Armbruster, T., Gnos, E., Dixon, R., Gutzmer, J., Hejny, C., Döbelin, N., and Medenbach, O. (2002) Manganvesuvianite and tweddillite, two new Mn^{3+}-silicate minerals from the Kalahari manganese fields, South Africa. Mineralogical Magazine, 66, 137–150.
Baur, H. (1974) The geometry of polyhedral distortions. Predictive relationships for the phosphate group. Acta Crystallographica, B30, 1195–1215.
Bermanec, V., Armbruster, T., Oberhänsli, R., and Zebec, V. (1994) Crystal chemistry of Pb- and REE-rich piemontite from Nezilovo, Macedonia. Schweizerische Mineralogische und Petrographische Mitteilungen, 74, 321–328.
Bish, D.L. and Reynolds, R.C. (1989) Sample preparation for X–ray diffraction. In D.L. Bish and J.E. Post, Eds., Reviews in Mineralogy: Modern powder diffraction, 20, 73–99. Mineralogical Society of America, Washington, D.C.
Bonazzi, P. and Menchetti, S. (1994) Structural variations induced by heat treatment in allanite and REE-bearing piemontite. American Mineralogist, 79, 1176–1184.
——— (1995) Monoclinic members of the epidote group: effects of the Al ↔ Fe^{3+} ↔ Fe^{2+} substitution and of the entry of REE^{3+}. Mineralogy and Petrology, 53, 133–153.
Bonazzi, P., Menchetti, S., and Palenzona, A. (1990) Strontiopiemontite, a new member of the epidote group from Val Graveglia, Liguria, Italy. European Journal of Mineralogy, 2, 519–523.
Bonazzi, P., Garbarino, C., and Menchetti, S. (1992) Crystal chemistry of piemontites: REE-bearing piemontite from Monte Brugiana, Alpi Apuane, Italy. European Journal of Mineralogy, 4, 23–33.
Burns, R.G. and Strens, R.G.J. (1967) Structural interpretation of polarized absorption spectra of the Al-Fe-Mn-Cr epidotes. Mineralogical Magazine, 36, 204–226.
Dollase, W.A. (1968) Refinement and comparison of the structures of zoisite and clinozoisite. American Mineralogist, 53, 1882–1898.
——— (1969) Crystal structure and cation ordering of piemontite. American Mineralogist, 54, 710–717.
——— (1971) Refinement of the crystal structures of epidote, allanite and hancockite. American Mineralogist, 56, 447–464.
——— (1973) Mössbauer spectra and iron distribution in the epidote-group minerals. Zeitschrift für Kristallographie, 138, 41–63.
——— (1986) Correction of intensities for preferred orientation in powder diffractometry: application of the March model. Journal of Applied Crystallography, 19, 267–272.
Enami, M. and Bannno, Y. (2001) Partitioning of Sr between coexisting minerals of the hollandite- and piemontite-groups in a quartz-rich schist from the Sanbagawa metamorphic belt, Japan. American Mineralogist, 86, 205–214
Fehr, K.T. and Heuss-Assbichler, S. (1997) Intracrystalline equilibria and immiscibility along the join clinozoisite-epidote: An experimental and ^{57}Fe Mössbauer study. Neues Jahrbuch für Minerlogie Abhandlungen, 172, 43–67.
Ferraris, G., Ivaldi, G., Fuess, H., and Gregson, D. (1989) Manganese/iron distribution in a strontian piemontite by neutron diffraction. Zeitschrift für Kristallographie, 187, 145–151.
Geller, S. (1971) Structures of α–Mn_2O_3, $(Mn_{0.983}Fe_{0.017})_2O_3$ and $(Mn_{0.37}Fe_{0.63})_2O_3$ and relation to magnetic ordering. Acta Crystallographica, B27, 821–828.
Giuli, G., Bonazzi, P., and Menchetti, S. (1999) Al-Fe disorder in synthetic epidotes: A single-crystal X-ray diffraction study. American Mineralogist, 84, 933–936.
Hill, R.J. and Flack, H.D. (1987) The use of the Durbin-Watson *d* statistic in Rietveld analysis. Journal of Applied Crystallography, 20, 356–361.
Ito, T., Morimoto, N., and Sadanaga, R. (1954) On the structure of epidote. Acta Crystallographica, 7, 53–59.
Izumi, F. (1993) Rietveld analysis program RIETAN and PREMOS and special applications. In R.A. Young, Ed., The Rietveld Method, pp. 236–253. Oxford Science Publications.
Izumi, F. and Ikeda, T. (2000) A Rietveld analysis program RIETAN-98 and its application to zeolites. Material Science Forum, 321–324.
Keskinen, M. and Liou, J.G. (1979) Synthesis and stability relations of Mn-Al piemontite, $Ca_2MnAl_2Si_3O_{12}(OH)$. American Mineralogist, 64, 317–328.
——— (1987) Stability relations of Mn-Fe-Al piemontite. Journal of Metamorphic Geology, 5, 495–507.
Kimura, Y. and Akasaka, M. (1999) Estimation of Fe^{2+}/Fe^{3+} and Mn^{2+}/Mn^{3+} rations by electron probe micro analyzer. Journal of the Mineralogical Society of Japan, 28, 159–166.
Kvick, A., Pluth, J.J., Richardson, J.W., and Smith, J.V. (1988) The ferric ion distribution and hydrogen bonding in epidote: a neutron diffraction study at 15 K. Acta Crystallographica, B44, 351–355.
Langer, K., Tillmanns, E., Kersten, M., Almen, H., and Arni, R.K. (2002) The crystal chemistry of Mn^{3+} in the clino- and orthozoisite structure types, $Ca_2M^{3+}{}_3[OH/O/SiO_4/Si_2O_7]$: A structural and spectroscopic study of some natural piemontites and "thulites" and their synthetic equivalents. Zeitschrift für Kristallographie, 217, 1–18.
Mottana, A. and Griffin, W.L. (1986) The crystal chemistry of piemontite from the type-locality (St. Marcel, Val d'Aosta, Italy). 13th General Meeting of the International Mineralogical Association, Varna, Bulgaria.
Myer, G.H. (1966) New data on zoisite and epidote. Americal Journal of Science, 264, 364–385.
Paesano, A., Kunrath, J.I., and Vasquez, A. (1983) A ^{57}Fe Mössbauer study of epidote. Hyperfine Interactions, 15/16, 841–844.
Post, J.E. and Bish, D.L. (1989) Rietveld refinement of crystal structures using powder X-ray diffraction data. In D.L. Bish and J.E. Post, Eds., Reviews in Mineralogy: Modern powder diffraction, 20, 277–308. Mineralogical Society of America, Washington, D.C.
Raudsepp, M., Hawthorne, F.C., and Turnock, A.C. (1990) Evaluation of the Rietveld method for the characterization of fine-grained products of mineral synthesis: the diopside-hedenbergite join. Canadian Mineralogist, 28, 93–109.
Robinson, K., Gibbs, G.V., and Ribbe, P.H. (1971) Quadratic elongation: a quantitative measure of distortion in coordination polyhedra. Science, 172, 567–570.
Strens, R.G.J. (1964) Synthesis and properties of piemontite. Nature, 201, 175–176.
Toraya, H. (1990) Array-type universal profile function for powder pattern fitting. Journal of Applied Crystallography, 23, 485–491.
Trojer, F.J. (1968) The crystal structure of parawollastonite. Zeitschrift für Kristallographie, 127, 291–308.
Young, R.A. (1993) Introduction to the Rietveld method. In R.A. Young, Ed., The Rietveld Method, p. 1–38. Oxford Science Publications.

Manuscript received November 18, 2003
Manuscript accepted February 10, 2004
Manuscript handled by Simona Quartieri